

## LONG-TERM SPECTRAL VARIABILITY OF THE ULTRA-LUMINOUS X-RAY SOURCE HOLMBERG IX X-1

V. JITHESH<sup>1</sup>, RANJEEV MISRA<sup>2</sup> AND ZHONGXIANG WANG<sup>1</sup>

<sup>1</sup> Shanghai Astronomical Observatory, Chinese Academy of Sciences, 80 Nandan Road, Shanghai 200030, China; jithesh@shao.ac.cn

<sup>2</sup> Inter-University Centre for Astronomy and Astrophysics, Post Bag 4, Ganeshkhind, Pune 411007, India

### ABSTRACT

We investigate the long-term spectral variability in the ultra-luminous X-ray source Holmberg IX X-1. By analyzing the data from eight *Suzaku* and 13 *XMM-Newton* observations conducted between 2001 and 2015, we perform a detailed spectral modeling for all spectra with simple models and complex physical models. We find that the spectra can be well explained by a disc plus thermal Comptonization model. Applying this model, we unveil correlations between the X-ray luminosity ( $L_X$ ) and the spectral parameters. Among the correlations, a particular one is the statistically significant positive correlation between  $L_X$  and the photon index ( $\Gamma$ ), while at the high luminosities of  $> 2 \times 10^{40}$  erg s<sup>-1</sup>, the source becomes marginally hard and that results a change in the slope of the  $\Gamma - L_X$  correlation. Similar variability behavior is observed in the optical depth of the source around  $L_X \sim 2 \times 10^{40}$  erg s<sup>-1</sup> as the source becomes more optically thick. We consider the scenario that a corona covers the inner part of the disc, and the correlations can be explained as to be driven by the variability of seed photons from the disc input into the corona. On the basis of the disc-corona model, we discuss the physical processes that are possibly indicated by the variability of the spectral parameters. Our analysis reveals the complex variability behavior of Holmberg IX X-1 and the variability mechanism is likely related to the geometry of the X-ray emitting regions.

*Keywords:* accretion, accretion discs – black hole physics – X-rays: binaries – X-rays: individual (Holmberg IX X-1)

### 1. INTRODUCTION

Ultra-luminous X-ray sources (ULXs) are extragalactic, point-like, non-nuclear X-ray sources with observed X-ray luminosity,  $L_X > 10^{39}$  erg s<sup>-1</sup>, exceeding the Eddington limit for a typical stellar-mass ( $\sim 10 M_\odot$ ) black hole (see [Feng & Soria 2011](#), for a review on ULXs). Studies with *Advanced Satellite for Cosmology and Astrophysics* (*ASCA*) observations ([Makishima et al. 2000](#)) revealed the X-ray flux variability on different time-scales, which suggests the binary accreting nature for ULXs. Early spectra of ULXs were described by a multi-color disc blackbody (MCD; [Mitsuda et al. 1984](#)) plus power law (PL) model, mimicking the popular spectral model for Galactic black hole X-ray binaries (BHXBs; See [Remillard & McClintock 2006](#)). Such modeling has provided evidence of cool thermal components ( $kT_{\text{in}} \sim 0.20$  keV; [Miller et al. 2003](#)), which has been interpreted as the existence of intermediate-mass black holes (IMBHs) of mass  $\sim 10^2 - 10^4 M_\odot$  in ULXs ([Colbert & Mushotzky 1999](#); [Coleman Miller & Colbert 2004](#)). However, this interpretation has been challenged by the highest quality *XMM-Newton* observations, where the observed spectra show a broad curvature ([Stobbart et al. 2006](#)) at high energies ( $\gtrsim 3$  keV), which does not correspond to any of the known sub-Eddington accretion states in BHXBs ([Remillard & McClintock 2006](#)) and is hardly reconciled

with the IMBH interpretation ([Roberts 2007](#)). The peculiar features (a soft component and the curvature at the high energies) in the highest quality data suggest a new observational state for ULXs, which is referred as *ultraluminous state* ([Gladstone et al. 2009](#)). Moreover, the observed properties of the ULXs are better explained on basis of disc plus Comptonized corona models in this state and such modeling suggests that the majority of ULXs are black holes of stellar origin accreting at near-Eddington and/or super-Eddington rate ([Stobbart et al. 2006](#); [Pintore & Zampieri 2012](#); [Sutton et al. 2013](#)). In addition, the recent discovery of pulsating neutron stars (NSs) in the three ULXs, M82 X-2 ([Bachetti et al. 2014](#)), NGC 5907 X-1 and NGC 7793 P13 ([Israel et al. 2017a,b](#)), has proved the existence of NSs as the compact primaries in the ULX population. It is also noted that typical ULX spectra can be described equally well with phenomenological models adopted for Galactic X-ray pulsars ([Pintore et al. 2017](#)). Thus a few non-pulsating ULXs may host NSs.

Spectral variability has been studied for individual as well as a sample of ULXs ([Feng & Kaaret 2006b, 2009](#); [Kajava & Poutanen 2009](#); [Pintore & Zampieri 2012](#)). In individual ULXs, the monitoring observations have been used to trace the long-term variability, which sometimes was interpreted as state transition ([Kubota et al. 2001](#); [Dewangan et al. 2004](#); [Godet et al.](#)

2009; Dewangan et al. 2010). The lower quality *ASCA* observations of two ULXs IC 342 X-1 and X-2 exhibited a canonical transition between low/hard and high/soft states (Kubota et al. 2001), where the two states were modeled with a PL and MCD component, respectively. However, there were flux variations not associated with any obvious state changes in some ULXs. For example, *Swift* monitoring observations of Holmberg II X-1, Holmberg IX X-1, NGC 5408 X-1 and NGC 4395 X-2 suggested that these ULXs remained in the same spectral states as their flux varied by an order of magnitude (Kaaret & Feng 2009; Grisé et al. 2010). Variability studies have also revealed several correlations between the spectral parameters, when fitting relatively low counting statistics spectra with a MCD plus PL model, especially the disc luminosity versus temperature and photon index versus X-ray luminosity ( $\Gamma - L_X$ ) correlations. Such correlations help compare the observed variations with the expectation from theoretical models. The disc luminosity versus temperature correlation,  $L_{\text{Disc}} \propto T^4$ , has been reported for several ULXs (Feng & Kaaret 2006b, 2009; Kajava & Poutanen 2009), when modeled with absorbed MCD, which show consistency with the prediction from the standard accretion disc model. However, other ULXs appear to follow an anti-correlation between the parameters,  $L_{\text{Disc}} \propto T_{\text{in}}^{-3.5}$ , when fitted with a cool MCD plus PL model (Feng & Kaaret 2007; Soria 2007; Kajava & Poutanen 2009). In addition, ULXs exhibited a  $\Gamma - L_X$  correlation when modeled with PL or MCD plus PL (Feng & Kaaret 2006b,a; Kajava & Poutanen 2008; Feng & Kaaret 2009; Kajava & Poutanen 2009, and reference therein). Such a correlation has already been observed in BHXBs and active galactic nuclei (Magdziarz et al. 1998; Zdziarski et al. 2002, 2003), and suggests that the variability mechanism is related to the geometry of the disc-corona in these sources (Haardt et al. 1997; Merloni & Fabian 2001).

The spectral variability studies of ULXs will thus help understand the geometry and physical processes in these systems, which can provide constraints on the nature of ULXs. A large number of available observations provide a unique opportunity for such studies on the nearby ULXs. In this paper, we present the long-term spectral variability study of the ULX Holmberg IX X-1 (hereafter Ho IX X-1) using the archival *Suzaku* and *XMM-Newton* observations. The data from the observations cover nearly the same energy range, 0.3–10 keV, and are in good quality, allowing us to test different spectral models thoroughly and identify the model for well describing the source emission. In our study, we used a two-component thermal model (disc blackbody plus thermal Comptonization), which has been found to be able to describe the spectral variability of ULXs quite well (Vierdayanti et al. 2010; Pintore & Zampieri 2012; Pintore et al. 2014; Luangtip et al. 2016). In section 1.1, we briefly explain Ho IX X-1 and its previous variability studies. The observations and data reduction method

are described in the §2. The analysis and results are presented in §3. The discussion is presented in §4.

### 1.1. Holmberg IX X-1 and the Variability Studies

Ho IX X-1 is one of the brightest ULXs with an average X-ray luminosity of  $\sim 10^{40}$  erg s $^{-1}$ . It is located near the galaxy M81 and is about 2 arcmin away from the irregular dwarf galaxy Holmberg IX. Since the discovery with *Einstein* observatory (Fabbiano 1989), the source has been studied with all major X-ray observatories (La Parola et al. 2001). The source was variable on time-scales of weeks to months and exhibited flux variations by a factor of seven in the *Swift* monitoring observations (Kaaret & Feng 2009). Apart from the X-ray flux variability, Ho IX X-1 is one of the few ULXs that exhibited mHz QPOs in the long *XMM-Newton* observation (Dewangan et al. 2006). The *XMM-Newton* spectra were modeled by the cool accretion disc ( $kT_{\text{in}} \sim 0.17 - 0.29$  keV) plus PL components and suggest an IMBH accretor of mass  $\sim 10^3 M_{\odot}$  by scaling with the measured disc temperatures (Miller et al. 2004). However, the *Swift* long-term monitoring observations of Ho IX X-1 (Kong et al. 2010) showed that the spectra can be described by the dual thermal model with cool blackbody and warm disc blackbody components. This model description leads to the suggestion that the accretor may be a  $10 M_{\odot}$  black hole accreting well above the Eddington limit or a  $100 M_{\odot}$  black hole at the Eddington rate. The broadband X-ray spectral study of Ho IX X-1, based on *Suzaku* and *XMM-Newton* observations, confirmed the earlier indication of the cut-off feature in the spectra of bright ULXs (Stobbart et al. 2006), which revealed the lack of an additional high-energy PL component that would otherwise contribute significantly to the X-ray emission (Dewangan et al. 2013). Later, the coordinated broadband X-ray observations performed with *NuSTAR*, *XMM-Newton* and *Suzaku* confirmed that the curvature observed previously in the limited bandpass is a true spectral cutoff (Walton et al. 2014).

Because Ho IX X-1 is one of the brightest nearby ULXs, its variability has been studied in the past. Earlier studies either used hardness ratios or the best-fitted disc plus PL model to investigate the spectral variability (La Parola et al. 2001; Wang 2002; Miller et al. 2004; Winter et al. 2007; Kaaret & Feng 2009). Vierdayanti et al. (2010) studied the variability of the source in detail with a disc plus thermal Comptonization (*comptt*) model. Using the *Swift* and limited number of *XMM-Newton* observations, they suggested a cool, optically thick Comptonizing corona for the source, which is consistent with the results reported in Gladstone et al. (2009). The observed variability is roughly characterized by a decrease in coronal electron temperature and an increase in the optical depth as the source becomes brighter.

The coordinated broadband X-ray observations of Ho IX X-1 with *NuSTAR*, *XMM-Newton* and *Suzaku* (Walton et al. 2014) revealed substantial spectral vari-

ability between two epochs of spectra (2012 October – November). The broadband spectra, in the 0.3–30 keV energy band, were well described either by two thermal models (`diskbb` and `diskpbb`) or disc-corona model (`diskbb+comptt`) along with a PL-like tail (`simpl`) at high energies. The source was observed at a brighter state in the second epoch, where the flux and temperature of one of the thermal component changed significantly compared to the first epoch in the two thermal model description. The spectral evolution of the source could be dominated either by the hot or cool temperature components, while both scenarios require highly non-standard behavior in the observed evolution. Recently, four coordinated broadband observations with *Suzaku* and *NuSTAR* expanded the broadband variability study (Walton et al. 2017) and showed similar spectral variability. Luangtip et al. (2016) studied the spectral evolution of Ho IX X-1 using the *Swift*, *NuSTAR*, and *XMM-Newton* observations. They found that the flat or two-component spectra in the 1–6 keV band at lower luminosities tend to evolve to a curved and disc-like spectrum at higher luminosities and the peak energy in the curved spectrum decreases with increase in luminosity. They suggest that a super-critical accretion disc with massive winds can explain this spectral evolution of the source.

## 2. OBSERVATIONS AND DATA REDUCTION

We used the observations of Ho IX X-1 obtained with *Suzaku* and *XMM-Newton*, which are publicly available, and analyzed the individual data in the 0.3–10 keV energy band. The list of the observations is given in Table 1.

### 2.1. *Suzaku*

Eight on-axis observations of Ho IX X-1 conducted with the *Suzaku* observatory (Mitsuda et al. 2007) were used for the analysis. We reduced the unfiltered *Suzaku* data using the standard software package, HEASOFT version 6.15.1, and reprocessed the X-ray imaging spectrometer (XIS) data using the specific HEADAS tool AEPIPELINE. The target was extracted from a circle of radius 220 arcsec in XIS0, XIS1 and XIS3, whereas the background events were selected from two circular regions near the target region with radius of 110 arcsec. The front illuminated (FI) CCDs spectra, XIS0 and XIS3, were added using the FTOOL ADDASCASPEC. The co-added spectra were then grouped with a minimum of 60–300 counts per bin, depending upon the quality of the data.

### 2.2. *XMM-Newton*

The *XMM-Newton* data were obtained from the *XMM-Newton* science archive and reduced using the standard tools of *XMM-Newton* Science Analysis Software (SAS) version 14.0. The data from the *XMM-Newton* European Photon Imaging Camera (EPIC) PN (Strüder et al. 2001) and metal oxide semiconductor

**Table 1.** Observation log in the chronological order

Data	ObsID	Date	Exposure (ksec)
<i>XMM1</i>	0111800101	2001 Apr 22	132.7
<i>XMM2</i>	0111800301	2001 Apr 22	8.0
<i>XMM3</i>	0112521001	2002 Apr 10	10.7
<i>XMM4</i>	0112521101	2002 Apr 16	11.5
<i>XMM5</i>	0200980101	2004 Sep 26	119.1
<i>XMM6</i>	0657802001	2011 Mar 24	27.5
<i>XMM7</i>	0657801601	2011 Apr 17	21.1
<i>XMM8</i>	0657801801	2011 Sep 26	25.4
<i>XMM9</i>	0657802201	2011 Nov 23	23.9
<i>Suzaku1</i>	707019010	2012 Apr 13	182.5
<i>Suzaku2</i>	707019020	2012 Oct 21	107.5
<i>XMM10</i>	0693850801	2012 Oct 23	14.1
<i>Suzaku3</i>	707019030	2012 Oct 24	106.9
<i>XMM11</i>	0693850901	2012 Oct 25	14.0
<i>Suzaku4</i>	707019040	2012 Oct 26	110.0
<i>XMM12</i>	0693851001	2012 Oct 27	13.9
<i>XMM13</i>	0693851701	2012 Nov 12	9.9
<i>XMM14</i>	0693851801	2012 Nov 14	13.8
<i>XMM15</i>	0693851101	2012 Nov 16	13.3
<i>Suzaku5</i>	709015010	2014 May 03	31.9
<i>Suzaku6</i>	709015020	2014 Nov 15	34.1
<i>Suzaku7</i>	709015030	2015 Apr 06	31.5
<i>Suzaku8</i>	709015040	2015 May 16	34.1

(MOS; Turner et al. 2001) detectors were used for the analysis. The full-field background light curve extracted from the EPIC camera in 10–12 keV energy range was used to select and remove the particle flaring background, and the good time intervals file was created. Out of fifteen *XMM-Newton* observations, two observations, *XMM2* and *XMM7* in Table 1, were highly affected by particle flaring and the available exposure time is too low to obtain good quality spectra. Thus, these observations were not included in the further analysis. We used the PN events with the best quality (FLAG = 0), PATTERN  $\leq$  4, and removed the hot pixels in the data by using the flag expression `#XMMEA_EP`, while FLAG = 0, PATTERN  $\leq$  12 and `#XMMEA_EM` expression were used for the MOS data. The source and background events were selected from a circular region of radius ranges of 35–45 arcsec; the different extraction radii were for the purpose of avoiding chip gaps. The background regions were extracted from a source-free region near the ULX and if possible, from the same CCD. In some of the observations, especially *XMM13*, *XMM14*, and *XMM15*, the source was bright enough for EPIC-MOS to be affected by mild pileup (see Walton et al. 2014). To reduce the pileup effects, we considered only single grade events in these observations. The source and background spectra in the 0.3–10 keV band, along with response and ancillary response files, were extracted from the clean filtered



event list using the standard *XMM-Newton* SAS tasks. All spectra were grouped to minimum counts of 30–300, depending upon the quality of the data.

### 3. ANALYSIS AND RESULTS

#### 3.1. Spectral Analysis

We performed detailed spectral modeling with simple models and complex physical models to understand the variability. The spectral modeling were performed with XSPEC version 12.8.1g (Arnaud 1996). We fitted the *Suzaku* and *XMM-Newton* (PN and MOS simultaneously) spectra in the 0.6–10 keV and 0.3–10 keV, respectively. In order to perform the spectral analysis in the same energy band, i.e., 0.3–10 keV, we extended the low-energy range of *Suzaku* data to 0.3 keV (using ENERGIES command in XSPEC) and derived the spectral parameters based on the best-fit models. Due to the calibration uncertainties, the 1.7–2 keV energy range was excluded from the *Suzaku* XIS spectra. The uncertainties on the best-fit parameters were quoted at a 90% confidence level. Two multiplicative absorption components (tbabs in XSPEC; Wilms et al. 2000) were used to incorporate the intervening absorption. The first component was fixed at the Galactic column  $N_{\text{H,Gal}} = 5.54 \times 10^{20} \text{ cm}^{-2}$  (Kalberla et al. 2005) towards the direction of the source, while the second component, which was free to vary, represents the absorption local to the ULX.

Initially, we fitted the spectra with an absorbed PL model. The model provides a statistically acceptable fit for only six spectra, where the null hypothesis probability  $> 0.05$ , and fails to explain the spectra from *XMM1* and *XMM5*, where the reduced  $\chi^2 > 2$  ( $\chi^2/\text{degrees of freedom (d.o.f)} = 651.6/323$  and  $1648.5/463$ , respectively; see Table 2). Thus, we added the MCD model (diskbb in XSPEC) to the PL. This combined model improved the fit significantly in majority of the spectra compared to the absorbed PL and the differences in the  $\chi^2$  values of the two models ranges from 1106.9 (obs. *XMM5*) to 1.2 (obs. *Suzaku5*) for the loss of two additional d.o.f (see Table 2). In addition, improved fits were obtained for *XMM1* and *XMM5* spectra ( $\chi^2/\text{d.o.f} = 582.4/321$  and  $541.6/461$ , respectively). We then attempted with an exponentially cut-off PL (cutoffpl) by replacing the PL component, which further improved the fit, especially for the *XMM-Newton* observations, though the cut-off energies ( $E_{\text{cutoff}} > 3 \text{ keV}$ ) were not well constrained in some of the cases. As pointed out in §1, the high energy cut-off or curvature commonly found in the bright ULXs can be described by thermal Comptonization in a cool and optically thick corona. Using thermal Comptonization models, comptt or nthcomp (in XSPEC), is appropriate in such circumstances. Thus, we tested these models by replacing the cutoffpl and both the models provide statistically acceptable fit to the spectra (see Table 2). While the former model is widely used to characterize the thermal Comptonization, here we proceeded with the nthcomp model to ex-

plain the observed spectral features.

The nthcomp model (Zdziarski et al. 1996; Życki et al. 1999) describes the thermal Comptonization in a relatively cool and optically thick plasma. The electron plasma temperature ( $kT_e$ ), photon index ( $\Gamma$ ) and seed photon temperature ( $kT_s$ ) are the free parameters of the model. The soft X-ray emission described by MCD is considered as the principal component, providing seed photons for the Comptonization. Thus, the temperatures of the MCD component ( $kT_{\text{in}}$ ) and the seed photons were kept the same and varied together. In the disc-corona models, if the optically thick corona masks the underneath disc, the seed photon temperature is not always equal to the disc temperature. We also repeated the analysis by disconnecting the two temperatures. However this assumption led to difficulties in finding a unique global minimum in the spectral fit (see also Feng & Kaaret 2009; Pintore & Zampieri 2012). Thus we decided to keep the two temperatures as the same. Because the tbabs  $\times$  tbabs  $\times$  (diskbb + nthcomp) model provides the acceptable best-fits and reasonable physical explanations, we considered it as the base-line model. All the spectra were fitted with this base-line model and the best-fit parameters are listed in Table 3. The total unabsorbed luminosity ( $L_X$ ) and the luminosity of disc component ( $L_{\text{Disc}}$ ) were calculated using the convolution model cflux available in XSPEC.

#### 3.2. Spectral Variability

We first investigated how the spectral parameters,  $N_{\text{H}}$ ,  $kT_{\text{in}}$ ,  $kT_e$ ,  $L_{\text{Disc}}$ , and  $\Gamma$ , changed with X-ray luminosity  $L_X$ . Their variations as a function of  $L_X$  are shown in Figure 1 and 2. From the figures, it is clear that the parameters exhibit an approximate trend with  $L_X$ . Among them, the plasma temperature ( $kT_e \sim 1-4 \text{ keV}$ ) has large uncertainties and was poorly constrained in some of the observations, although it first increases, and then decrease as  $L_X$  increases. The disc luminosity  $L_{\text{Disc}}$  is in the range of a few times  $10^{39} \text{ erg s}^{-1}$  with large uncertainties and not well constrained in some of the observations. Thus, we can consider  $L_{\text{Disc}}$  not strongly variable or relatively stable in these observations. The photon index  $\Gamma$  varies significantly with  $L_X$  (Figure 2). It first has a strong correlation with  $L_X$ , but turns to be lower at the highest  $L_X$ .

We quantified the correlations between the X-ray luminosity and the best-fit parameters by obtaining the Spearman rank correlation coefficient ( $r_s$ ) and the probability ( $p$ -value) for the null hypothesis. If the  $p$ -value is 0.05 or less, the correlation is considered to be significant. The parameters  $N_{\text{H}}$  and  $\Gamma$  are positively correlated with  $L_X$ , where  $r_s = 0.53$  ( $p = 1.43 \times 10^{-2}$ ) and  $r_s = 0.52$  ( $p = 1.51 \times 10^{-2}$ ), respectively. The parameter  $kT_{\text{in}}$  is negatively correlated with both  $L_X$  and  $L_{\text{Disc}}$ , where  $r_s = -0.58$  ( $p = 5.57 \times 10^{-3}$ ) and  $r_s = -0.61$  ( $p = 3.41 \times 10^{-3}$ ), respectively. However, the parameters  $L_{\text{Disc}}$  and  $kT_e$  do not show any significant correla-

**Table 2.** The obtained  $\chi^2/\text{d.o.f}$  for different models

Data	Model 1	Model 2	Model 3	Model 4	Model 5
<i>XMM1</i>	651.6/323	582.4/321	399.5/320	388.6/320	393.2/320
<i>XMM3</i>	347.4/288	277.7/286	267.2/285	269.1/285	269.6/285
<i>XMM4</i>	373.4/323	318.4/321	316.4/320	315.5/320	316.2/320
<i>XMM5</i>	1648.5/463	541.6/461	467.2/460	463.4/460	463.4/460
<i>XMM6</i>	279.0/230	224.9/228	224.3/227	224.3/227	224.4/227
<i>XMM8</i>	384.5/321	377.9/319	376.8/318	373.6/318	373.8/318
<i>XMM9</i>	438.7/392	433.7/390	397.7/389	398.8/389	399.8/389
<i>Suzaku1</i>	417.4/346	403.2/344	359.2/343	356.7/343	357.1/343
<i>Suzaku2</i>	346.5/289	331.6/287	313.3/286	311.0/286	312.8/286
<i>XMM10</i>	388.1/303	317.3/301	316.5/300	315.7/300	316.0/300
<i>Suzaku3</i>	315.0/300	303.0/298	300.1/297	300.1/297	301.0/297
<i>XMM11</i>	388.6/331	319.0/329	314.5/328	313.1/328	313.8/328
<i>Suzaku4</i>	345.8/359	332.3/357	326.7/356	326.9/356	327.1/356
<i>XMM12</i>	354.1/301	334.3/299	320.5/298	319.3/298	318.8/298
<i>XMM13</i>	498.6/366	440.5/364	363.8/363	377.6/363	378.4/363
<i>XMM14</i>	572.9/381	511.2/379	380.2/378	379.7/378	380.1/378
<i>XMM15</i>	454.9/333	421.2/331	370.2/330	374.7/330	374.5/330
<i>Suzaku5</i>	294.4/271	293.2/269	288.3/268	288.2/268	287.2/268
<i>Suzaku6</i>	261.6/253	252.9/251	233.7/250	224.3/250	224.4/250
<i>Suzaku7</i>	295.4/248	279.9/246	275.0/245	276.0/245	275.9/245
<i>Suzaku8</i>	267.6/246	266.3/244	266.3/243	265.6/243	266.0/243

NOTE—Model 1:  $\text{tbabs} \times \text{tbabs} \times \text{powerlaw}$ ; Model 2:  $\text{tbabs} \times \text{tbabs} \times (\text{diskbb} + \text{powerlaw})$ ; Model 3:  $\text{tbabs} \times \text{tbabs} \times (\text{diskbb} + \text{cutoffpl})$ ; Model 4:  $\text{tbabs} \times \text{tbabs} \times (\text{diskbb} + \text{compTT})$ ; Model 5:  $\text{tbabs} \times \text{tbabs} \times (\text{diskbb} + \text{nthcomp})$ .

tion with  $L_X$  and the coefficients are  $r_s = 0.31$  ( $p = 0.17$ ) and  $r_s = -0.30$  ( $p = 0.18$ ), respectively.

We note that  $N_H$  is positively correlated with  $L_X$ . If the correlation has a physical origin, the increasing luminosity is a signature of the denser environment, while a non-physical origin is due to the degeneracy between  $N_H$  and  $\Gamma$  in model fitting, artificially boosting the unabsorbed luminosity (see more details in [Kajava & Poutanen 2009](#)). For some of the ULXs,  $N_H$  is also correlated with  $\Gamma$ , when fitted with a PL or a disc plus PL model ([Feng & Kaaret 2009](#); [Kajava & Poutanen 2009](#)). However, we did not find an  $N_H$ - $\Gamma$  correlation for Ho IX X-1 with the base-line model. This result is consistent with that in [Kajava & Poutanen \(2009\)](#), where the  $N_H$  -  $\Gamma$  correlation no longer exists when fitted with the PL plus cool MCD model. Since  $N_H$  varies marginally with  $L_X$ , we tried to fix the absorption column to their mean value ( $N_H = 1.34 \times 10^{21} \text{ cm}^{-2}$ ) and fitted the spectra again. The spectral fits were worse for the cases where the best-fit values of  $N_H$  differ from the mean value, but we found that the  $\Gamma$ - $L_X$  correlation still appears. Thus, although we considered the local absorption column as a free parameter in the base-line model, this choice did not affect the correlation (for a given spectrum, higher  $N_H$  can cause higher  $\Gamma$  and higher  $L_X$ ).

Examining the correlation between  $\Gamma$  and  $L_X$  (Figure 2),  $\Gamma$  reaches  $\sim 1.8$  around the luminosity of  $2 \times 10^{40} \text{ erg s}^{-1}$  and actually turns to be lower with values

of  $\sim 1.6$ - $1.7$  at higher luminosities. We investigated this plausible turn-over feature by fitting a line to all data points first. A poor fit with a reduced  $\chi^2$  of 3.6 (19 d.o.f) was obtained. Excluding the data points above the luminosity of  $2 \times 10^{40} \text{ erg s}^{-1}$ , then the fitting was improved to have a reduced  $\chi^2$  of 1.0 (13 d.o.f). This improvement is significant at a 99.95% confidence level compared to the first fit, indicating the presence of the turn-over. We also attempted a broken power law fit for the  $\Gamma$  and  $L_X$  correlation. The fitting identified a break at  $1.99 \pm 0.10 \times 10^{40} \text{ erg s}^{-1}$  with a reduced  $\chi^2$  of  $\sim 1.7$  for 17 d.o.f, and the slopes were  $0.27 \pm 0.04$  and  $-0.17 \pm 0.05$  below and above the break respectively. The fit results further support a turn-over around  $\sim 2 \times 10^{40} \text{ erg s}^{-1}$ .

Many ULXs, when their spectra were fitted with a PL plus cool MCD model, exhibited an anti-correlation between the disc luminosity and temperature,  $L_{\text{Disc}} \propto T_{\text{in}}^{-3.5}$  ([Soria 2007](#); [Kajava & Poutanen 2009](#)). This anti-correlation suggests that the ULXs considered in those work were in a state of having high-accretion rate and low-disc temperature (ultraluminous branch; [Soria 2007](#)). We checked the correlation between  $L_{\text{Disc}}$  and  $kT_{\text{in}}$  derived from the base-line model, and the anti-correlation appears to be consistent with the previous reported results ([Soria 2007](#); [Kajava & Poutanen 2009](#)).

The X-ray luminosity of Ho IX X-1 has changed by a factor of  $\sim 3 - 4$  during these observations and among them, *XMM5* and *Suzaku6* data have the lowest flux.

**Table 3.** Best-fit parameters for the base-line model and the derived parameters from `nthcomp` model function

Data	$N_{\text{H}}$	$kT_{\text{in}}$	$\Gamma$	$kT_{\text{e}}$	$\log L_{\text{X}}$	$\log L_{\text{Disc}}$	$\chi^2/\text{d.o.f}$	$\log L_{\text{Input}}$	$A$
<i>XMM1</i>	$0.19^{+0.01}_{-0.01}$	$0.20^{+0.01}_{-0.01}$	$1.72^{+0.01}_{-0.01}$	$> 1.39$	$40.41^{+0.01}_{-0.01}$	$39.41^{+0.03}_{-0.03}$	393.2/320	39.83	3.90
<i>XMM3</i>	$0.12^{+0.03}_{-0.03}$	$0.27^{+0.05}_{-0.04}$	$1.66^{+0.06}_{-0.08}$	$2.38^{+0.74}_{-0.38}$	$40.10^{+0.03}_{-0.03}$	$39.36^{+0.10}_{-0.11}$	269.6/285	39.44	4.65
<i>XMM4</i>	$0.17^{+0.04}_{-0.04}$	$0.21^{+0.05}_{-0.03}$	$1.81^{+0.04}_{-0.06}$	$> 2.56$	$40.21^{+0.05}_{-0.04}$	$39.39^{+0.21}_{-0.18}$	316.2/320	39.61	4.46
<i>XMM5</i>	$0.13^{+0.01}_{-0.01}$	$0.24^{+0.01}_{-0.01}$	$1.55^{+0.02}_{-0.02}$	$2.45^{+0.16}_{-0.13}$	$40.05^{+0.01}_{-0.01}$	$39.38^{+0.04}_{-0.04}$	463.4/460	39.26	6.25
<i>XMM6</i>	$0.15^{+0.06}_{-0.05}$	$0.25^{+0.06}_{-0.04}$	$1.61^{+0.06}_{-0.09}$	$> 2.18$	$40.17^{+0.06}_{-0.05}$	$39.52^{+0.18}_{-0.15}$	224.4/227	39.43	6.05
<i>XMM8</i>	$0.13^{+0.05}_{-0.03}$	$0.23^{+0.11}_{-0.08}$	$1.83^{+0.05}_{-0.04}$	$> 3.01$	$40.30^{+0.05}_{-0.03}$	$< 39.20$	373.8/318	39.79	3.97
<i>XMM9</i>	$0.14^{+0.04}_{-0.03}$	$0.25^{+0.08}_{-0.06}$	$1.80^{+0.03}_{-0.04}$	$2.22^{+0.32}_{-0.23}$	$40.42^{+0.03}_{-0.02}$	$39.02^{+0.31}_{-1.67}$	399.8/389	39.91	3.68
<i>Suzaku1</i>	$< 0.09$	$0.30^{+0.10}_{-0.08}$	$1.64^{+0.03}_{-0.05}$	$2.57^{+0.25}_{-0.12}$	$40.16^{+0.04}_{-0.02}$	$38.91^{+0.28}_{-0.29}$	357.1/343	39.55	4.76
<i>Suzaku2</i>	$< 0.19$	$0.21^{+0.12}_{-0.04}$	$1.70^{+0.04}_{-0.04}$	$2.76^{+0.45}_{-0.29}$	$40.23^{+0.09}_{-0.06}$	$39.18^{+0.47}_{-0.87}$	312.7/286	39.59	5.05
<i>XMM10</i>	$0.14^{+0.04}_{-0.03}$	$0.24^{+0.05}_{-0.04}$	$1.68^{+0.04}_{-0.06}$	$> 2.56$	$40.21^{+0.04}_{-0.03}$	$39.40^{+0.16}_{-0.14}$	316.0/300	39.54	5.43
<i>Suzaku3</i>	$< 0.17$	$0.23^{+0.16}_{-0.11}$	$1.75^{+0.04}_{-0.04}$	$3.03^{+0.75}_{-0.37}$	$40.23^{+0.10}_{-0.03}$	$< 39.55$	301.0/297	39.67	4.58
<i>XMM11</i>	$0.13^{+0.03}_{-0.03}$	$0.28^{+0.06}_{-0.05}$	$1.68^{+0.05}_{-0.07}$	$2.94^{+1.78}_{-0.59}$	$40.24^{+0.03}_{-0.02}$	$39.43^{+0.10}_{-0.11}$	313.8/328	39.60	4.80
<i>Suzaku4</i>	$0.17^{+0.09}_{-0.12}$	$0.17^{+0.06}_{-0.05}$	$1.80^{+0.04}_{-0.05}$	$3.45^{+1.53}_{-0.59}$	$40.33^{+0.11}_{-0.10}$	$39.53^{+0.39}_{-0.90}$	327.1/356	39.70	4.81
<i>XMM12</i>	$0.10^{+0.04}_{-0.03}$	$0.31^{+0.10}_{-0.08}$	$1.67^{+0.09}_{-0.15}$	$2.16^{+0.53}_{-0.36}$	$40.24^{+0.04}_{-0.03}$	$39.39^{+0.17}_{-0.18}$	318.8/298	39.63	4.13
<i>XMM13</i>	$0.22^{+0.09}_{-0.13}$	$0.16^{+0.28}_{-0.03}$	$1.73^{+0.06}_{-0.05}$	$1.88^{+0.18}_{-0.13}$	$40.52^{+0.12}_{-0.10}$	$< 40.08$	378.4/363	39.89	4.59
<i>XMM14</i>	$0.17^{+0.06}_{-0.05}$	$0.20^{+0.07}_{-0.03}$	$1.62^{+0.04}_{-0.03}$	$1.66^{+0.11}_{-0.09}$	$40.51^{+0.06}_{-0.04}$	$39.43^{+0.36}_{-0.51}$	380.0/378	39.84	4.91
<i>XMM15</i>	$0.22^{+0.09}_{-0.09}$	$0.17^{+0.07}_{-0.02}$	$1.67^{+0.06}_{-0.06}$	$1.72^{+0.20}_{-0.14}$	$40.56^{+0.11}_{-0.08}$	$39.68^{+0.46}_{-1.18}$	374.5/330	39.87	4.86
<i>Suzaku5</i>	$< 0.15$	$0.39^{+0.12}_{-0.29}$	$1.65^{+0.09}_{-0.17}$	$2.63^{+1.01}_{-0.55}$	$40.15^{+0.11}_{-0.01}$	$< 39.46$	287.2/268	39.59	4.20
<i>Suzaku6</i>	$< 0.13$	$0.36^{+0.14}_{-0.10}$	$1.44^{+0.10}_{-0.20}$	$1.96^{+0.30}_{-0.29}$	$40.05^{+0.05}_{-0.02}$	$39.28^{+0.15}_{-0.19}$	224.4/250	39.29	5.69
<i>Suzaku7</i>	$0.25^{+0.17}_{-0.19}$	$0.19^{+0.08}_{-0.03}$	$1.61^{+0.07}_{-0.08}$	$2.62^{+1.18}_{-0.47}$	$40.18^{+0.22}_{-0.15}$	$39.70^{+0.45}_{-0.61}$	275.8/245	39.32	6.27
<i>Suzaku8</i>	$< 0.35$	$< 0.48$	$1.81^{+0.06}_{-0.06}$	$> 2.41$	$40.20^{+0.22}_{-0.14}$	$< 40.07$	266.0/243	39.59	5.05

NOTE—(1) Data; (2) neutral hydrogen column density in units of  $10^{22} \text{ cm}^{-2}$ ; (3) inner disc temperature in keV; (4) photon index; (5) electron temperature in keV; (6) - (7) logarithmic total unabsorbed 0.3–10 keV X-ray luminosity and the luminosity of disc component in  $\text{erg s}^{-1}$ , calculated by assuming the distance of 3.4 Mpc (Hill et al. 1993); (8)  $\chi^2$  statistics and degrees of freedom; (9) logarithmic luminosity of input seed photons in  $\text{erg s}^{-1}$ ; (10) amplification factor. Seed photon temperature,  $kT_{\text{S}} = kT_{\text{in}}$  and input type = 1.

During the observations conducted in 2012 November (*XMM13* – *XMM15*), the source was observed with the highest X-ray luminosity ( $L_{\text{X}} \sim 3.6 \times 10^{40} \text{ erg s}^{-1}$ ) compared to the other observations. The MCD component appears relatively less variable and the flux contribution from it is always less ( $\lesssim 33\%$ ) than that from the Comptonized component in all observations. Thus, the observed variability is dominated by the Comptonization process.

Our base-line model with a black hole suggests that the compact object is surrounded by the corona and multi-color accretion disc, where the inner region of the disc may be covered by the corona. The input seed photons from the accretion disc are injected into the corona and the corona Comptonizes these seed photons. Since the source exhibits variability, it is important to know how the changes occur in the radiation mechanism and geometry of the source. Using the XSPEC model function (*nthcomp.f*) for the `nthcomp` model, we estimated the amplification factor,  $A = L_{\text{C}}/L_{\text{Input}}$ , where  $L_{\text{C}}$  and  $L_{\text{Input}}$  are the luminosities of the Comptonizing cloud and the input seed photons, respectively. The parameter  $L_{\text{Input}}$  depends on the luminosity of the disc as well as the fraction of input seed photons seen by the corona. Moreover, the fraction of input seed photons entering the corona depends on the accretion geometry of the

system. We derived  $A$ ,  $L_{\text{C}}$ , and  $L_{\text{Input}}$  from the model function for all the spectra using the best-fit parameters. The variations of the derived parameters with  $L_{\text{X}}$  are shown in Figure 3.

It is clear from the figures that  $L_{\text{Input}}$  and  $L_{\text{C}}$  increase with  $L_{\text{X}}$ . Moreover,  $L_{\text{Input}}$  varies more rapidly (by a factor of  $\sim 5$ ) than  $L_{\text{C}}$  (a factor of  $\sim 3$ ) and it appears to be flat ( $\sim 7 \times 10^{39} \text{ erg s}^{-1}$ ) at the highest  $L_{\text{X}}$ . The changes in  $L_{\text{Input}}$  and  $L_{\text{C}}$  lead to the variations of  $A$ , which decreases from 6.3 to 3.7 as  $L_{\text{X}}$  increases, but then turns to be  $\sim 4.5 - 5$  at the highest luminosity (Figure 3). In the Comptonization context,  $\Gamma$  is inversely proportional to  $A$ . We did observe such variability in the case of Ho IX X–1, where the source evolves from hard ( $\Gamma \sim 1.4$ ) to soft ( $\Gamma \sim 1.8$ ) as  $A$  decreases. We also estimated the optical depth  $\tau$  (Zdziarski et al. 1998) as,

$$\tau = \left( \frac{kT_{\text{e}}}{m_{\text{e}}c^2} \right)^{-1/2} \left[ \left( \Gamma + \frac{1}{2} \right)^2 - \frac{9}{4} \right]^{-1/2} \quad (1)$$

The derived  $\tau$  values are consistent with having optically thick corona ( $\tau \sim 6 - 13$ ) and showed marginal variations with  $L_{\text{X}}$ , first dropping and then going up as  $L_{\text{X}}$  increases.

#### 4. DISCUSSION

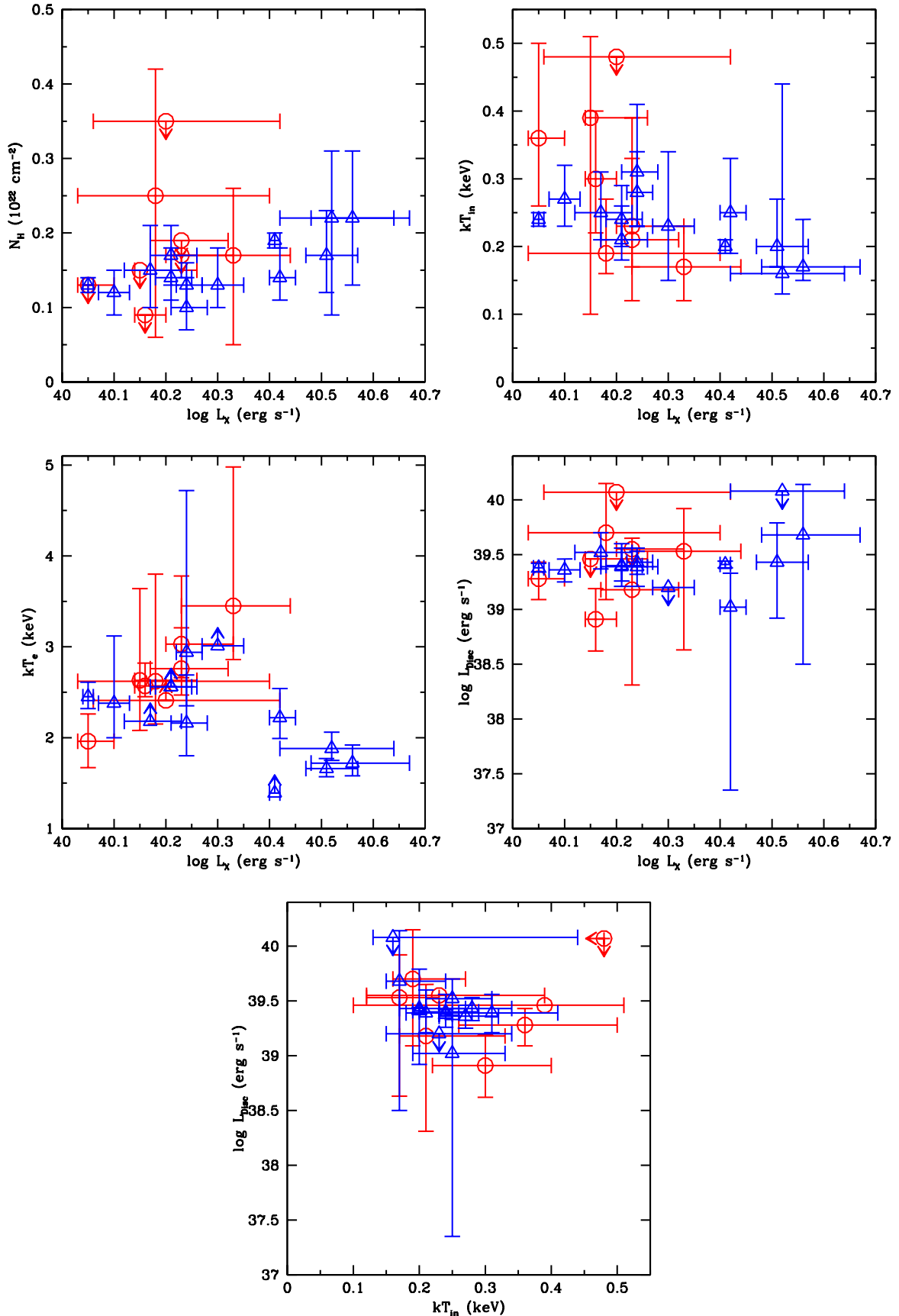


**Figure 1.** The variations of best-fit spectral parameters ( $N_{\text{H}}$ ,  $kT_{\text{in}}$  and  $kT_e$ ) with X-ray luminosity ( $L_X$  and  $L_{\text{Disc}}$ ) in the 0.3–10 keV energy band. The red open circles and blue triangles represent the *Suzaku* and *XMM-Newton* data respectively.

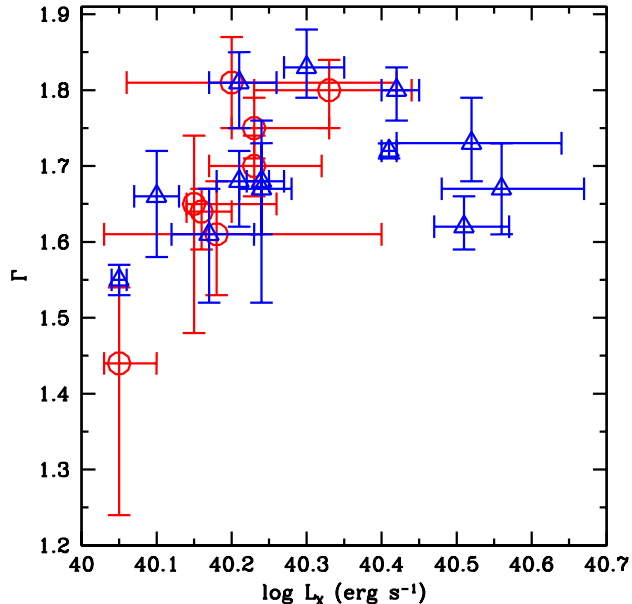


**Figure 2.** Photon index versus X-ray luminosity for Ho IX X-1 obtained from the base-line model. The red open circles and blue triangles represent the *Suzaku* and *XMM-Newton* spectra respectively.

We analyzed the *Suzaku* and *XMM-Newton* observations of the bright ULX Ho IX X-1 conducted over a period of  $\sim 14$  years, to study its spectral variability. We systematically studied the spectra with different models. The data were better represented by a MCD plus thermal Comptonization (`nthcomp`) model. The best-fit spectral parameters derived from this model were consistent with the results of broadband spectral studies in the 0.3–30 keV energy band using the disc-corona plus PL-like tail model ( $N_{\text{H}} \sim 1.4 \times 10^{21} \text{ cm}^{-2}$ ,  $kT_{\text{in}} \sim 0.3$  keV,  $kT_{\text{e}} \sim 2.4$  keV; Walton et al. 2014). Using the MCD plus thermal Comptonization model, we studied the variability behavior of the accretion disc plus corona as a function of X-ray luminosity. Our analysis revealed that the best-fit model parameters showed strong trends with X-ray luminosity. The parameters  $N_{\text{H}}$  and  $\Gamma$  were found to be positively correlated with X-ray luminosity, while  $kT_{\text{in}}$  was negatively correlated. The plasma temperature derived from this model description ranges  $\sim 1 - 4$  keV, consistent with the low temperature, optically thick corona seen in other ULXs (Stobbart et al. 2006; Gladstone et al. 2009). Moreover,  $kT_{\text{e}}$  did not show a statistically significant correlation with  $L_{\text{X}}$ , although it marginally varied with  $L_{\text{X}}$ . The parameter  $\Gamma$  significantly varied with  $L_{\text{X}}$  and exhibited a statistically significant positive correlation. It evolved from hard ( $\Gamma \sim 1.4$ ) to soft ( $\Gamma \sim 1.8$ ) as  $L_{\text{X}}$  increases, while at higher X-ray luminosities  $\Gamma$  turned to be slightly lower ( $\Gamma \sim 1.7$ ). In these observations, the X-ray luminosity of Ho IX X-1 varied by a factor of  $\sim 3 - 4$  and the flux contribution from the Comptonized component was much higher than that from the disc component.

In the MCD plus thermal Comptonization model, one can assume a geometry, where a standard cold accretion disc is truncated at radius  $R_{\text{tr}}$  and the inner region contains hot plasma. The plasma Comptonizes the seed photons from the outer disc, and the fraction of input seed photons that enter the plasma region is related to a solid angle subtending between the plasma region and the outer disc. For this geometry, the input seed photon luminosity must be smaller than the disc luminosity,  $L_{\text{Input}}/L_{\text{Disc}} \lesssim 1$ , but if  $L_{\text{Input}} \ll L_{\text{Disc}}$ , it poses an unphysically small solid angle. This geometry has been proposed for the ULX NGC 1313 X-1, where the source was at a low flux state (Dewangan et al. 2010). For Ho IX X-1, such geometry is consistent with the spectra of *XMM5*, *XMM6* and *Suzaku7*, where  $L_{\text{Input}}/L_{\text{Disc}} \sim 0.4 - 0.8$ . The values suggest the solid angle  $\Delta\Omega \sim (0.4 - 0.8) \times 2\pi$ . The estimated truncation radius from the normalization of the disc component for these three spectra ranges between  $8.7 \times 10^8 - 2.1 \times 10^9 \text{ cm}$ , which is corrected for color factor  $\kappa = 1.7$  (Shimura & Takahara 1995; the inclination angle of the binary is assumed to be  $60^\circ$ ). The proposed scenario is consistent with the existence of a massive black hole of mass about  $50 - 200 M_{\odot}$ . If we assume a mass of  $200 M_{\odot}$  for Ho IX X-1, the Schwarzschild radius would be  $r_{\text{s}} = 2GM/c^2 \sim 6 \times 10^7 \text{ cm}$ , making the transition radius  $R_{\text{tr}} \sim 15 - 35 r_{\text{s}}$ . Thus, the three spectra were consistent with a model where a massive black hole surrounded by a standard accretion disc truncated at a radius of  $\sim 15 - 35 r_{\text{s}}$ .

However, majority of the spectra, 18 out of 21, appear to be inconsistent with this geometry as  $L_{\text{Input}} > L_{\text{Disc}}$ . The observed properties of the source instead can be explained by an alternative geometry, the “sandwich model” (Liang & Price 1977; Haardt & Maraschi 1993; Svensson & Zdziarski 1994), which has been successful in describing the observed properties of Galactic BHBs (Kubota & Done 2004; Done & Kubota 2006, and references therein). In this model, the corona covers the standard accretion disc and takes some fraction of the total gravitational power, while the remaining fraction is dissipated in the disc. The corona Comptonizes the seed photons from the underlying disc and a fraction of Comptonized photons ( $\xi$ ) impinge on the disc, and get absorbed. This geometry is valid only when the fraction  $\xi$  is less than the maximum value ( $\xi < \xi_{\text{max}} = 1/A$ ). Such geometry can explain the observed properties of NGC 1313 X-1 in the high flux state (Dewangan et al. 2010), where the corona covers the entire disc. For Ho IX X-1, the MCD component is clearly evident in all the spectra, suggesting that the corona covers only the inner part of the disc. This can be confirmed by estimating the size of the corona region  $R_{\text{c}}$ . Assuming the input seed photon luminosity as a blackbody,  $\sigma T_{\text{s}}^4 2\pi R_{\text{c}}^2 = L_{\text{Input}}$  (see also Dewangan et al. 2010, for more details), where  $T_{\text{s}}$  is the temperature of the disc. The derived values of  $R_{\text{c}}$  exhibit an increasing trend with  $L_{\text{X}}$  (see Figure 3) and  $R_{\text{c}} \sim 1.4 - 13.6 \times 10^8 \text{ cm}$ , which can definitely mask



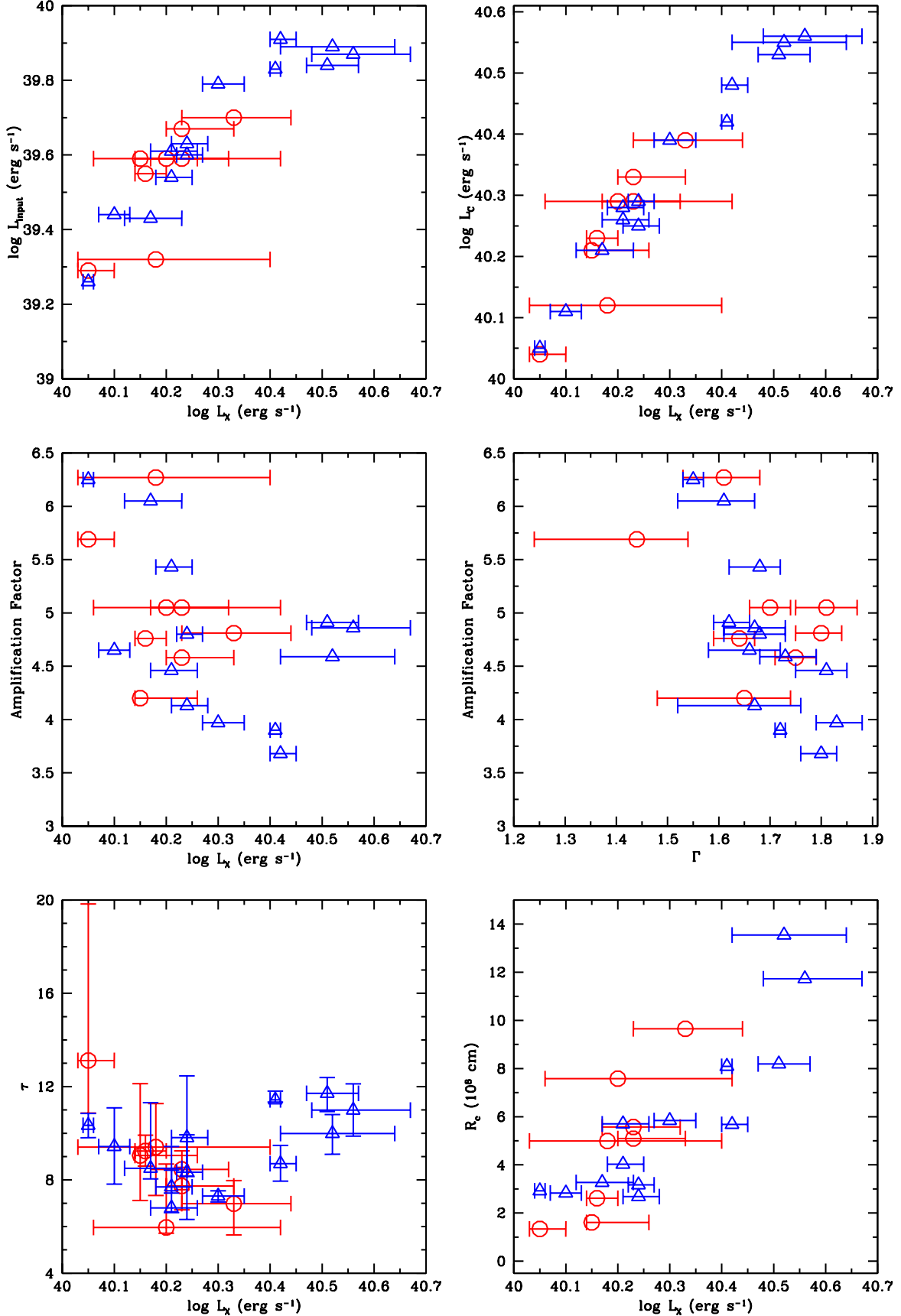


**Figure 3.** *Top and middle panels* : The variations of derived parameters from the *nthcomp* model function with  $L_X$  and  $\Gamma$ . *Bottom panels* : The variations of optical depth and coronal radius with  $L_X$ . The colors and symbols are the same as those used in Figure 1. See text for more details.

the inner part of the disc. The negative correlation between  $kT_{\text{in}}$  and  $L_X$  (see Figure 1) can thus be because of the larger part of the inner disc covered by the corona.

From our studies, we revealed the existence of a more complex  $\Gamma - L_X$  relation:  $\Gamma$  evolves from hard to soft ( $\sim 1.4$  to  $1.8$ ) as  $L_X$  increases, while at higher  $L_X$ ,  $\Gamma$  turns to be slightly harder ( $\sim 1.7$ ). The positive  $\Gamma - L_X$  correlation has been reported for Ho IX X-1, based on an absorbed PL fit, with limited sample of observations (Kajava & Poutanen 2009). The observed values of photon index ( $\Gamma \sim 1.5 - 2.0$ ) from the simple PL are also consistent with that from our base-line model. We further note that the  $\Gamma - L_X$  correlation has been reported for several other ULXs, for example, NGC 1313 X-1 (Feng & Kaaret 2006b), Antennae X-11 (Feng & Kaaret 2006a), NGC 253 X-4, IC 342 X-6, Holmberg II X-1, NGC 5204 X-1 and NGC 5408 X-1 (Feng & Kaaret 2009; Kajava & Poutanen 2009), in which their spectra were fitted with a PL or a MCD plus PL model. This correlation phase of ULXs was explained as an intermediate state with hybrid properties from the thermal and steep PL states (Feng & Kaaret 2009).

However in the disc-corona model we used, the  $\Gamma - L_X$  correlation can be explained as due to the process of the thermal Comptonization of the seed photons from the accretion disc by the hot corona (Zdziarski et al. 2003, and references therein). In this process, the seed photons are variable, and when the seed photon flux increases, the X-ray emission becomes softer and stronger (Zdziarski & Grandi 2001; Zdziarski et al. 2002). Therefore in this model, the variability of  $L_{\text{Input}}$  should be stronger than that of  $L_C$ . Ho IX X-1 is likely such a case. We found that  $L_{\text{Input}}$  is more variable (by a factor of  $\sim 5$ ) than  $L_C$  and the amplification factor decreases with  $L_X$ . Moreover, the input seed photon flux for Ho IX X-1 shows the sign of saturation at high luminosities. Thus, at high luminosities although the radiation flux from the corona has increased, the seed photon flux remains more or less same, which should lead to hardening of the spectra as is marginally observed. The saturation of the seed photon flux implies that while the coronal radiative power has increased, the disc flux remained nearly constant or did not increase proportionally. This suggests that at high luminosities a larger fraction of the accretion energy is dissipated in the corona as compared to disc, perhaps because the corona has become larger, covering a greater fraction of the accretion disc. The variable seed photon flux also affects the coronal parameters. Our modeling showed a marginal increase in  $kT_e$  as  $L_X$  (or  $L_{\text{Input}}$ ) increases, while it drops at the high luminosity. The former behavior has been observed in other ULXs, NGC 5204 X-1 and Holmberg II X-1 (Roberts et al. 2006; Feng & Kaaret 2009), while the latter is consistent with earlier studies of Ho IX X-1 (Vierdayanti et al. 2010) and IC 342 X-1 (Feng & Kaaret 2009). The change in  $kT_e$  is also reflected in the optical depth, which first decreases (from

$\tau \sim 13$  to  $6$ ) and then becomes very thick ( $\tau \sim 12$ ) at the high luminosity. The variability indicates that Ho IX X-1 exhibits a cooler ( $kT_e \sim 2$  keV) and very thick corona ( $\tau \sim 12$ ) at different luminosity values. We note that in NGC 1313 X-2, the different corona states (‘very-thick’ and ‘thick’) correlate with luminosity and the source becomes more luminous in the ‘very-thick’ state (Pintore & Zampieri 2012). The comparison indicates the more complex variability behavior in Ho IX X-1.

As mentioned above, the source turns to be marginally hard at the high luminosities, i.e.,  $L_X > 2 \times 10^{40}$  erg s $^{-1}$ . This turn-over of  $\Gamma$  in the  $\Gamma - L_X$  plane is significant, and results a change in the slope of the correlation. Interestingly, the optical depth also exhibits similar variability pattern as the source appears to be optically very thick ( $\tau \sim 12$ ) above the luminosity  $2 \times 10^{40}$  erg s $^{-1}$ . In Pintore et al. (2014), the softening behavior was observed for Ho IX X-1 in the ‘thick’ state as the intensity increases in the hardness-intensity diagram (left panel of Figure 6 in Pintore et al. 2014). We also observe such softening variability behavior below the luminosity  $2 \times 10^{40}$  erg s $^{-1}$  (mostly in the ‘thick’ state) in the  $\Gamma - L_X$  plane. However, the behavior of low-luminosity sources (NGC 253 X-1 and NGC 1313 X-2 in the ‘thick’ state; Pintore et al. 2014) is different, where these sources become marginally hard as the intensity increases to a level consistent with the ‘very thick’ state seen in a few ULXs. Then in the ‘very-thick’ state, NGC 1313 X-2 turns to have the softening behavior as the intensity increases. Thus, comparing Ho IX X-1 to NGC 1313 X-2, these sources have different behavior below and above a certain luminosity threshold. The threshold is also different in the two sources, as for the former, its value is  $\sim 2 \times 10^{40}$  erg s $^{-1}$ , while it can be approximated to be  $5 \times 10^{39}$  erg s $^{-1}$  (see Figure 3 in Pintore & Zampieri 2012) for the latter.

In the models with a corona, the energy balance is achieved by adjusting the coronal parameters: varying either the electron temperature alone or both  $kT_e$  and  $\tau$ . For example, if the optical depth is constant, the corona adjusts the electron temperature itself to the variable seed photon flux. Thus, the energy balance is satisfied by an increased cooling of the plasma ( $kT_e$  decreases), which results in the increase of  $\Gamma$  and softer spectrum (Zdziarski & Grandi 2001; Zdziarski et al. 2002, 2003). However, it is also possible that the variation in the photon index is due to the optical depth variation (Svensson 1994; Haardt et al. 1997, and reference therein). In such cases, the energy balance is satisfied by adjusting  $\tau$  and the softening of the spectrum is associated with an increase of  $kT_e$  (Nicastro et al. 2000; Chiang 2002; Zdziarski et al. 2003). The latter explanation seems to be consistent with observed behavior of the coronal parameters of Ho IX X-1 below a luminosity of  $2 \times 10^{40}$  erg s $^{-1}$ . At the luminosity above  $2 \times 10^{40}$  erg s $^{-1}$ , the reason for the change in the slope of the  $\Gamma - L_X$  relation appears to be the saturation of

the input seed photon luminosity. Considering this and the energy balance of the system in the high luminosity, one would expect that at constant optical depth the coronal electron temperature increases as  $L_X$  increases, while we observed an opposite behavior. Thus, this behavior can be explained as when  $L_X$  increases above  $2 \times 10^{40}$  erg s $^{-1}$ , the corona becomes not only more energetic but also more mass loaded, which increases the coronal density and the optical depth of the source. In such a case, the decrease in the mean energy per scattering is largely compensated by an increase of the average number of scatterings, which produces the observed hardening of the spectrum.

While in this work, we have interpreted Ho IX X-1 as a massive black hole accreting at near-Eddington rate, the source has also been interpreted as a stellar-mass black hole accreting at super-critical rates leading to a strong radiation driven winds (Sutton et al. 2013; Pintore et al. 2014; Luangtip et al. 2016). In this scenario, the wind may be sufficiently dense and cover a large fraction of the outer disc. When a ULX system is observed face-on, the inner region around a black hole emits a hard spectrum, and at high inclination angles, the line-of-sight passes through the outer, cold region of the wind and a softer spectrum is observed (see e.g. Middleton et al. 2011; Sutton et al. 2013; Middleton et al. 2014). Sutton et al. (2013) studied the spectral variability of a large sample of ULXs, using a doubly absorbed MCD plus PL model, and empirically classified the ULX population into three spectral regimes, referred as *broadened-disc*, *hard ultraluminous*, and *soft ultraluminous*. These spectral states can be explained as being due to different viewing angles to the sources. However, Ho IX X-1 shows spectral characteristics of the *hard ultraluminous* and *broadened-disc* class at different times (Sutton et al. 2013). This was confirmed by another detailed study of large sample of ULXs, where color-color and hardness-intensity diagrams were used (Pintore et al. 2014). Luangtip et al. (2016) also characterized the spectral evolution of Ho

IX X-1 below 10 keV. They used a two-thermal component model, `diskbb+comptt`, similar to what has been used in this work and our results are consistent with theirs. For example, the flux variations primarily came from the hard component and at the high-luminosity end, the spectra of the hard component is harder. The difference between theirs and this work is in the interpretation of the spectral variability, where they consider the wind model of a stellar-mass black hole, while here we consider the system to be a massive black hole accreting at near-Eddington rates. We note that no direct evidence for a strong disc wind has been found in Ho IX X-1 (Walton et al. 2012, 2013), although some residuals in the source's soft spectra have been suggested to be line features from the wind (Middleton et al. 2015). In any case, our study has revealed interesting variability features of the source, in particular the  $\Gamma - L_X$  correlation. These features can be considered as significant constraints, to be explained by any scenario proposed for this ULX.

#### ACKNOWLEDGEMENTS

We thank the anonymous referee for the constructive comments and suggestions that improved this manuscript. This research has made use of data obtained from the High Energy Astrophysics Science Archive Research Center (HEASARC), provided by NASA's Goddard Space Flight Center. This research was supported by the National Program on Key Research and Development Project (Grant No. 2016YFA0400804) and the National Natural Science Foundation of China (11373055, 11633007). VJ acknowledges the IUCAA Visitor's Program and the financial support from Chinese Academy of Sciences through President's International Fellowship Initiative (CAS PIFI, Grant No. 2015PM059). Z.W. acknowledges the support by the CAS/SAFEA International Partnership Program for Creative Research Teams.

*Software:* HEASOFT (v 6.15.1), SAS (v 14.0), XSPEC (v 12.8.1g; Arnaud 1996)

#### REFERENCES

- Arnaud, K. A. 1996, in *Astronomical Society of the Pacific Conference Series*, Vol. 101, *Astronomical Data Analysis Software and Systems V*, ed. G. H. Jacoby & J. Barnes, 17
- Bachetti, M., Harrison, F. A., Walton, D. J., et al. 2014, *Nature*, 514, 202
- Chiang, J. 2002, *ApJ*, 572, 79
- Colbert, E. J. M., & Mushotzky, R. F. 1999, *ApJ*, 519, 89
- Coleman Miller, M., & Colbert, E. J. M. 2004, *International Journal of Modern Physics D*, 13, 1
- Dewangan, G. C., Griffiths, R. E., & Rao, A. R. 2006, *ApJL*, 641, L125
- Dewangan, G. C., Jithesh, V., Misra, R., & Ravikumar, C. D. 2013, *ApJL*, 771, L37
- Dewangan, G. C., Misra, R., Rao, A. R., & Griffiths, R. E. 2010, *MNRAS*, 407, 291
- Dewangan, G. C., Miyaji, T., Griffiths, R. E., & Lehmann, I. 2004, *ApJL*, 608, L57
- Done, C., & Kubota, A. 2006, *MNRAS*, 371, 1216
- Fabbiano, G. 1989, *ARA&A*, 27, 87
- Feng, H., & Kaaret, P. 2006a, *ApJ*, 653, 536
- . 2006b, *ApJL*, 650, L75
- . 2007, *ApJL*, 660, L113
- . 2009, *ApJ*, 696, 1712
- Feng, H., & Soria, R. 2011, *NewAR*, 55, 166
- Gladstone, J. C., Roberts, T. P., & Done, C. 2009, *MNRAS*, 397, 1836
- Godet, O., Barret, D., Webb, N. A., Farrell, S. A., & Gehrels, N. 2009, *ApJL*, 705, L109
- Grisé, F., Kaaret, P., Feng, H., Kajava, J. J. E., & Farrell, S. A. 2010, *ApJL*, 724, L148
- Haardt, F., & Maraschi, L. 1993, *ApJ*, 413, 507
- Haardt, F., Maraschi, L., & Ghisellini, G. 1997, *ApJ*, 476, 620
- Hill, J. K., Gessner, S. E., Bohlin, R. C., et al. 1993, *ApJL*, 402, L45

- Israel, G. L., Belfiore, A., Stella, L., et al. 2017a, *Science*, 355, 817
- Israel, G. L., Papitto, A., Esposito, P., et al. 2017b, *MNRAS*, 466, L48
- Kaaret, P., & Feng, H. 2009, *ApJ*, 702, 1679
- Kajava, J. J. E., & Poutanen, J. 2008, in *American Institute of Physics Conference Series*, Vol. 1054, American Institute of Physics Conference Series, ed. M. Axelsson, 39–47
- Kajava, J. J. E., & Poutanen, J. 2009, *MNRAS*, 398, 1450
- Kalberla, P. M. W., Burton, W. B., Hartmann, D., et al. 2005, *A&A*, 440, 775
- Kong, A. K. H., Yang, Y. J., Yen, T.-C., Feng, H., & Kaaret, P. 2010, *ApJ*, 722, 1816
- Kubota, A., & Done, C. 2004, *MNRAS*, 353, 980
- Kubota, A., Mizuno, T., Makishima, K., et al. 2001, *ApJL*, 547, L119
- La Parola, V., Peres, G., Fabbiano, G., Kim, D. W., & Bocchino, F. 2001, *ApJ*, 556, 47
- Liang, E. P. T., & Price, R. H. 1977, *ApJ*, 218, 247
- Luangtip, W., Roberts, T. P., & Done, C. 2016, *MNRAS*, 460, 4417
- Magdziarz, P., Blaes, O. M., Zdziarski, A. A., Johnson, W. N., & Smith, D. A. 1998, *MNRAS*, 301, 179
- Makishima, K., Kubota, A., Mizuno, T., et al. 2000, *ApJ*, 535, 632
- Merloni, A., & Fabian, A. C. 2001, *MNRAS*, 328, 958
- Middleton, M. J., Sutton, A. D., & Roberts, T. P. 2011, *MNRAS*, 417, 464
- Middleton, M. J., Walton, D. J., Roberts, T. P., & Heil, L. 2014, *MNRAS*, 438, L51
- Middleton, M. J., Walton, D. J., Fabian, A., et al. 2015, *MNRAS*, 454, 3134
- Miller, J. M., Fabbiano, G., Miller, M. C., & Fabian, A. C. 2003, *ApJL*, 585, L37
- Miller, J. M., Fabian, A. C., & Miller, M. C. 2004, *ApJ*, 607, 931
- Mitsuda, K., Inoue, H., Koyama, K., et al. 1984, *PASJ*, 36, 741
- Mitsuda, K., Bautz, M., Inoue, H., et al. 2007, *PASJ*, 59, 1
- Nicastro, F., Piro, L., De Rosa, A., et al. 2000, *ApJ*, 536, 718
- Pintore, F., & Zampieri, L. 2012, *MNRAS*, 420, 1107
- Pintore, F., Zampieri, L., Wolter, A., & Belloni, T. 2014, *MNRAS*, 439, 3461
- Pintore, F., Zampieri, L., Stella, L., et al. 2017, *ApJ*, 836, 113
- Remillard, R. A., & McClintock, J. E. 2006, *ARA&A*, 44, 49
- Roberts, T. P. 2007, *Ap&SS*, 311, 203
- Roberts, T. P., Kilgard, R. E., Warwick, R. S., Goad, M. R., & Ward, M. J. 2006, *MNRAS*, 371, 1877
- Shakura, N. I., & Sunyaev, R. A. 1973, *A&A*, 24, 337
- Shimura, T., & Takahara, F. 1995, *ApJ*, 445, 780
- Soria, R. 2007, *Ap&SS*, 311, 213
- Stobbart, A.-M., Roberts, T. P., & Wilms, J. 2006, *MNRAS*, 368, 397
- Strüder, L., Briel, U., Dennerl, K., et al. 2001, *A&A*, 365, L18
- Sutton, A. D., Roberts, T. P., & Middleton, M. J. 2013, *MNRAS*, 435, 1758
- Svensson, R. 1994, *ApJS*, 92, 585
- Svensson, R., & Zdziarski, A. A. 1994, *ApJ*, 436, 599
- Turner, M. J. L., Abbey, A., Arnaud, M., et al. 2001, *A&A*, 365, L27
- Vierdayanti, K., Done, C., Roberts, T. P., & Mineshige, S. 2010, *MNRAS*, 403, 1206
- Walton, D. J., Miller, J. M., Reis, R. C., & Fabian, A. C. 2012, *MNRAS*, 426, 473
- Walton, D. J., Miller, J. M., Harrison, F. A., et al. 2013, *ApJL*, 773, L9
- Walton, D. J., Harrison, F. A., Grefenstette, B. W., et al. 2014, *ApJ*, 793, 21
- Walton, D. J., Fürst, F., Harrison, F. A., et al. 2017, *ApJ*, 839, 105
- Wang, Q. D. 2002, *MNRAS*, 332, 764
- Wilms, J., Allen, A., & McCray, R. 2000, *ApJ*, 542, 914
- Winter, L. M., Mushotzky, R. F., & Reynolds, C. S. 2007, *ApJ*, 655, 163
- Zdziarski, A. A., & Grandi, P. 2001, *ApJ*, 551, 186
- Zdziarski, A. A., Johnson, W. N., & Magdziarz, P. 1996, *MNRAS*, 283, 193
- Zdziarski, A. A., Lubiński, P., Gilfanov, M., & Revnivtsev, M. 2003, *MNRAS*, 342, 355
- Zdziarski, A. A., Poutanen, J., Mikolajewska, J., et al. 1998, *MNRAS*, 301, 435
- Zdziarski, A. A., Poutanen, J., Paciesas, W. S., & Wen, L. 2002, *ApJ*, 578, 357
- Życki, P. T., Done, C., & Smith, D. A. 1999, *MNRAS*, 309, 561